Assessment of pilot direct contact membrane distillation regeneration of lithium chloride solution in liquid desiccant air-conditioning systems using computer simulation

Submitted to

Environmental Science and Pollution Research

Hung Cong Duong[1,2,*], Long Duc Nghiem[2], Ashley Joy Ansari[3], Thao Dinh Vu[1], and Khai Manh Nguyen[4]

[1] School of Environmental Engineering, Le Quy Don Technical University, Hanoi, Vietnam

[2] Centre for Technology in Water and Wastewater, School of Civil and Environmental Engineering, University of Technology, Sydney, Broadway, NSW 2007, Australia

[3] Strategic Water Infrastructure Laboratory, School of Civil Mining and Environmental Engineering, University of Wollongong, Wollongong, NSW 2522, Australia

[4] Faculty of Environmental Sciences, University of Science, Vietnam National University, Hanoi 334 Nguyen Trai, Thanh Xuan, Hanoi, Vietnam

* Corresponding author:

Hung Cong Duong, email: hungduongcong@gmail.com; Tel: +84 357 593 243

Abstract: Membrane distillation (MD) has been increasingly explored for treatment of various hyper saline waters, including lithium chloride (LiCl) solutions used in liquid desiccant air-conditioning (LDAC) systems. In this study, the regeneration of liquid desiccant LiCl solution by a pilot direct contact membrane distillation (DCMD) process is assessed using computer simulation. Unlike previous experimental investigations, the simulation allows to incorporate both temperature and concentration polarisation effects in the analysis of heat and mass transfer through the membrane, thus enabling the systematic assessment of the pilot DCMD regeneration of the LiCl solution. The simulation results demonstrate distinctive profiles of water flux, thermal efficiency, and LiCl concentration along the membrane under co-current and counter-current flow modes, and the pilot DCMD process under counter-current flow is superior to that under co-current flow regarding the process thermal efficiency and LiCl concentration enrichment. Moreover, for the pilot DCMD regeneration of LiCl solution under the counter-current flow, the feed inlet temperature, LiCl concentration, and especially the membrane leaf length exert profound impacts on the process performance: the process water flux halves from 12 to 6 L/(m^2·h) while thermal efficiency decreases by 20% from 0.46 to 0.37 when the membrane leaf length increases from 0.5 to 1.5 m.

Keywords: membrane distillation (MD); direct contact membrane distillation (DCMD); polarisation effects; heat and mass transfer, liquid desiccant air-conditioning (LDAC); liquid desiccant regeneration.

Declarations

Ethics approval and consent to participate

Not applicable

Consent for publication

Not applicable

Availability of data and materials

The datasets generated and/or analysed during the current study are not publicly available due to regulations of the funding but are available from the corresponding author on reasonable request.

Competing interests

The authors declare the following financial interests/personal relationships which may be considered as potential competing interests: Vietnam National Foundation for Science and Technology Development (NAFOSTED); Le Quy Don Technical University; University of Technology, Sydney

Funding

This research is funded by Vietnam National Foundation for Science and Technology Development (NAFOSTED) under the grant number 105.08-2019.08.

Authors' contributions

HCD: Conceptualisation, Methodology, Software, Formal Analysis, Resources, Writing-Original Draft;

LDN: Conceptualisation, Methodology, Review & Editing

AJA: Methodology, Validation, Formal Analysis

TDV: Validation, Writing, Review & Editing

KMN: Methodology, Validation, Formal Analysis, Review & Editing

1. Introduction

Membrane distillation (MD), a hybrid thermal-driven separation process, has been increasingly explored for treatment of various hyper saline waters due to its distinguishing attributes (Nguyen et al. 2018; Abdelkader et al. 2019; Duong et al. 2019). In the MD process, a hydrophobic microporous membrane is used to separate a saline water feed from a fresh distillate stream. Given its hydrophobic nature, the membrane retains liquid water on the feed side, but allows the transfer of water vapour through its pores to the other side, hence concentrating the feed water. The driving force for the transfer of water in the MD process is not the hydraulic and/or osmotic pressure difference but the water vapour pressure gradient induced by a temperature difference across the membrane. As a result, unlike pressure-driven membrane processes, MD is less subject to salt concentration of the feed water, and hence it is workable with various hyper saline waters including concentrated brine from reverse osmosis (RO) desalination (Yan et al. 2017; Bindels et al. 2020), diluted draw solution from forward osmosis (FO) (Nguyen et al. 2018), and liquid desiccant solutions used in air-conditioning industry (Duong et al. 2019; Zhou et al. 2020; Liu et al. 2021). Because only water vapour and volatile compounds are allowed to permeate through its membrane, the MD process can achieve theoretically complete salt rejections, enabling the regeneration and/or recovery of valuable dissolved salts in saline waters. More importantly, as a thermal-driven separation technology, the MD process can be powered by low-grade waste heat or renewable solar thermal energy to reduce the process energy cost. Given these notable attributes, MD has emerged as an ideal candidate to be integrated into other process for treatment of hyper saline waters with improved energy efficiency. One notable example can be the integration of MD into the liquid desiccant air-conditioning (LDAC) process (Duong et al. 2017; Duong et al. 2018; Lefers et al. 2018; Zhou et al. 2020; Zhou et al. 2020).

LDAC is a potential game changer in advancing the air-conditioning industry to become greener and more energy-efficient (Gurubalan et al. 2019; Chen et al. 2020; Salikandi et al. 2021). Currently, most conventional air-conditioning systems are based on the vapour compression process, whereby the air is first dehumidified by deep cooling to dew point temperature to condense moisture and then reheated to achieve a desired temperature. The deep cooling and the subsequent reheating of the air waste energy, rendering the conventional air-conditioning systems energy-inefficient (Modi and Shukla 2018; Duong et al. 2019). On the other hand, LDAC systems

dehumidify and cool the air via the direct absorption of moisture into a liquid desiccant solution (i.e. lithium chloride (LiCl) solution). The hygroscopic nature of the liquid desiccant solution drives the moisture removal without the need for deep cooling and reheating the air; therefore, the energy consumption of the LDAC systems is markedly reduced compared to that of the conventional vapour-compression based air-conditioners (Gurubalan et al. 2019; Chen et al. 2020; Salikandi et al. 2021).

Regeneration of liquid desiccant solution is a key step of the LDAC process (Duong et al. 2018; Lefers et al. 2018; Zhou et al. 2020). The moisture holding capacity (i.e. hygroscopicity) of the liquid desiccant solution depends on concentration and temperature. During the air dehumidification of the LDAC process, moisture absorption dilutes and warms the liquid desiccant solution, hence gradually reducing its hygroscopicity. To restore the liquid desiccant solution's hygroscopicity and hence the LDAC process's air dehumidification efficiency, the diluted (i.e. weak) liquid desiccant solution needs to be regenerated (i.e. reconcentrated and cooled) in a regenerator. Most current LDAC systems rely on thermal evaporation for the regeneration of liquid desiccant solutions (Cheng and Zhang 2013; Duong et al. 2019). This regeneration method involves heating the diluted liquid desiccant solution to a high temperature prior to spraying it in counter-current flow with a hot air stream in a packed bed media (Lowenstein 2008; Cheng and Zhang 2013; Salikandi et al. 2021). The direct contact between the hot liquid desiccant solution and the air stream inevitably leads to the carry-over of desiccant droplets in the air stream, which is regarded as a vexing technical issue of the thermal evaporation regeneration method (Duong et al. 2019; Gurubalan et al. 2019; Chen et al. 2020; Salikandi et al. 2021). Moreover, high-temperature heating required for the regeneration of liquid desiccant solution in the evaporation regenerator primarily contributes to the high energy consumption of the LDAC process. As a result, novel regeneration methods that are resistant to desiccant carry-over and workable at mild temperature are urgently needed for the realisation of LDAC systems. In this context, the MD process can be tapped into given its complete salt rejection and workability with hyper saline waters at mild temperature.

Previous experimental works have been conducted to prove the technical feasibility of MD for the regeneration of liquid desiccant solutions used in the LDAC process (Duong et al. 2017; Duong et al. 2018; Lefers et al. 2018; Zhou et al. 2019; Zhou et al. 2020; Zhou et al. 2020; Liu et al. 2021). Most notably, Duong et al. (2017) experimentally investigated the direct contact membrane

distillation (DCMD) regeneration of liquid desiccant LiCl solutions and proved that the DCMD process could regenerate the liquid desiccant LiCl solution of 29% without any issue of desiccant carry-over at the feed temperature of 65 °C. Zhou et al. (2020) systematically examined the performance of vacuum membrane distillation (VMD) during the regeneration of LiCl solution. Despite using short hollow fibre membranes (i.e. 0.52 m in length), the lab-scale VMD process could increase the concentration of the LiCl 20% solution by 0.2% when operating in the single-pass mode at the feed temperature of 65 °C (Zhou et al. 2020). Particularly, the experimental results demonstrated the profound impacts of LiCl solution temperature and membrane length on the regeneration performance of the VMD process.

Previous lab-scale experimental works have demonstrated the viability of MD regeneration of liquid desiccant LiCl solutions. It is, however, necessary to underline that there have been no experimental investigations or simulation studies on pilot or large-scale MD regeneration of liquid desiccant solutions, despite a great number of pilot MD processes experimentally demonstrated and simulated for seawater desalination applications (Hitsov et al. 2015; Dong et al. 2017; Duong et al. 2017; Andrés-Mañas et al. 2018; Andrés-Mañas et al. 2020). To facilitate the realisation of MD regeneration of liquid desiccant solutions, pilot or large-scale studies are of vital importance. Therefore, this study aims to assess a pilot MD process for regeneration of liquid desiccant LiCl solution with the aid of computer simulation. Unlike previous simulations of pilot seawater MD desalination, the pilot DCMD simulation model reported in this study incorporates the influences of the LiCl solution hyper salinity and the negative effects of polarisation phenomena, particularly the concentration polarisation, on the process mass and heat transfer. Given its flexibility and high accuracy, the simulation package offers useful means to elucidate the mass and heat transfer inside the pilot DCMD membrane module, thus allowing to elaborate the impacts of process operating conditions and membrane module specifications on the process performance during the regeneration of liquid desiccant LiCl solution.

2. Heat and mass transfer calculations and simulation approaches

2.1. Heat and mass transfer calculations

During the DCMD regeneration of LiCl solution, the transfer of water (i.e. mass transfer) occurs simultaneously with the heat flux through the membrane. While the mass transfer directly controls

157 the moisture desorption and hence the regeneration of the LiCl solution, the heat flux through the
158 membrane is undesirable as it reduces the driving force of the regeneration process. The mass
159 transfer through the membrane is proportional to the water vapour pressure difference between the
160 two sides of the membrane, and is expressed as (Alkhudhiri et al. 2012):

161 $$J = C_m \times \left(P_{m.f} - P_{m.d} \right) \quad (1)$$

162 where J is water flux (kg/(m^2·h)); C_m is the membrane mass transfer coefficient (kg/(m^2·h·Pa)); and
163 $P_{m.f}$ and $P_{m.d}$ are the water vapour pressures (Pa) at the feed and distillate membrane surfaces,
164 respectively. C_m, a function of membrane characteristics and process operating conditions, is
165 calculated as below (Alkhudhiri et al. 2012):

166 $$C_m = \left[\frac{3}{2} \frac{\tau\delta}{\varepsilon r} \left(\frac{\pi RT}{8M} \right)^{1/2} + \frac{\tau\delta}{\varepsilon} \frac{P_a}{PD} \frac{RT}{M} \right]^{-1} \quad (2)$$

167 where δ, ε, τ, and r are the membrane thickness (m), porosity (dimensionless), pore tortuosity
168 (dimensionless), and pore radius (m), respectively; M is the molecular weight of water (kg/mol); R
169 is the gas constant (i.e. 8.314 J/(mol·K)); T is the mean water vapour temperature (K) inside the
170 membrane pore; P and P_a are the total pressure and the air partial pressure (Pa) inside the membrane
171 pore; and D is the water diffusion coefficient (m^2/s). The distillate water vapour pressure at the
172 membrane surface (i.e. $P_{m.d}$) can be calculated using the Antoine equation (Alkhudhiri et al. 2012):

173 $$P_{m.d} = exp(23.1964 - \frac{3816.44}{T_{m.d} - 46.13}) \quad (3)$$

174 where $T_{m.d}$ is the distillate temperature (K) at the membrane surface. On the other hand, the
175 calculation of water vapour pressure at the feed membrane surface (i.e. $P_{m.f}$) involves complex
176 functions of LiCl solution concentration and temperature at the feed membrane surface (e.g. $S_{m.f}$
177 and $T_{m.f}$). More details of the water vapour pressure calculation of the LiCl solution at high
178 concentrations are provided elsewhere (Conde 2004; Duong et al. 2020).

179 During the DCMD process of the LiCl solution, in tandem with water vapour flux, heat is
180 transferred from the feed to the distillate via conduction through the membrane matrix and the

latent heat associated with the transferred water vapour. The heat flux (Q) through the membrane is described as (Alkhudhiri et al. 2012):

$$Q = \frac{k_m}{\delta}\left(T_{m.f} - T_{m.d}\right) + J\Delta H_v \tag{4}$$

where Q is in kJ/(m^2·h); k_m is the membrane thermal conductivity (W/(m·K)) and ΔH_v is the latent heat of evaporation of water (kJ/kg). The membrane thermal conductivity is a function of polymer thermal conductivity (k_s) and gas thermal conductivity (k_g), expressed as (Alkhudhiri et al. 2012):

$$k_m = \left[\frac{\varepsilon}{k_g} + \frac{1-\varepsilon}{k_s}\right]^{-1} \tag{5}$$

The latent heat of water evaporation (i.e. ΔH_v) is a function of the mean water vapour temperature inside the membrane pore, and is calculated as (Alkhudhiri et al. 2012):

$$\Delta H_v = 1.7535T + 2024.3 \tag{6}$$

Water flux calculation using the membrane mass transfer coefficient (C_m) in Eq. (1) involves temperature and salt concentration at the membrane surfaces (e.g. $T_{m.f}$, $T_{m.d}$, and $S_{m.f}$). During the DCMD process of LiCl solutions, polarisation effects cause the temperature and salt concentration at the membrane surfaces different to those in the bulk feed and distillate streams (e.g. $T_{b.f}$, $T_{b.d}$, and $S_{b.f}$) (Kuang et al. 2019; Anvari et al. 2020). While the bulk temperature and salt concentration of the feed and distillate streams can be experimentally measured, the measurements of these parameters at the membrane surfaces require complex instruments and impractical membrane module designs (Kuang et al. 2019; Lokare et al. 2019). In this context, several studies have utilised the process mass transfer coefficient (i.e. K_m) together with the bulk feed and distillate temperature and salt concentration for water flux calculation. This water flux calculation is more practical when involving the measurable thermodynamic properties of the bulk feed and distillate; however, it fails to incorporate polarisation effects, particularly concentration polarisation, resulting in considerable deviations between the calculated and experimentally measured water flux (Duong et al. 2017; Duong et al. 2018). The computer model developed for the simulation of the pilot DCMD process of seawater reported by Duong et al. (2017) includes the temperature polarisation effect in water

flux calculation, but deliberately neglects the concentration polarisation effect given the negligible impacts of seawater salinity on water flux. For the pilot DCMD regeneration of liquid desiccant LiCl solutions, the hyper salinity of the feed exerts profound influences on water flux; therefore, the concentration polarisation effect must be incorporated in water flux calculation together with the temperature polarisation effect.

The simulation model built for this study incorporates both temperature and concentration polarisation effects in water flux calculation and heat transfer analysis. Initially, water flux (J) is calculated using the bulk thermodynamic properties of the feed and distillate, then the temperature and LiCl concentration at the feed and distillate membrane surfaces (i.e. $T_{m.f}$, $S_{m.f}$, and $T_{m.d}$) are calculated as below (Khayet et al. 2004; Hitsov et al. 2015):

$$T_{m.f} = \frac{T_{b.f}h_f + h_m\left(T_{b.d} + T_{b.f}\frac{h_f}{h_d}\right) - J\Delta H_v}{h_f\left(1+\frac{h_m}{h_d}\right)+h_m} \tag{7}$$

$$T_{m.d} = \frac{T_{b.d}h_d + h_m\left(T_{b.f} + T_{b.d}\frac{h_d}{h_f}\right) + J\Delta H_v}{h_d\left(1+\frac{h_m}{h_f}\right)+h_m} \tag{8}$$

$$S_{m.f} = S_{b.f} \times \exp\left(\frac{J}{\rho \times k}\right) \tag{9}$$

where h_m, h_f, and h_d are respectively the heat transfer coefficient across the membrane and in the feed and distillate thermal boundary layers; ρ and k are the density and the water transfer coefficient of the LiCl solution feed. The heat transfer coefficient across the membrane (h_m) is dependent on the membrane thermal conductivity (k_m) and the membrane thickness (δ), while the calculations of the heat transfer coefficients in the feed and distillate boundary layers (h_f and h_d) involve Nusselt number (Nu), Reynolds number (Re), and Prandtl number (Pr) using the fluid thermodynamic properties (e.g. density, dynamic viscosity, specific heat capacity, and cross flow velocity) and the hydraulic diameter of the feed and distillate channels. Empirical equations for the calculations of

the thermodynamic properties of the LiCl solution feed and the distillate are provided in (Conde 2004). The calculated $T_{m.f}$, $T_{m.d}$, and $S_{m.f}$ are then used for the calculation of J in equation (1). The new calculated value is now assigned to J in the calculation of new $T_{m.f}$, $T_{m.d}$, and $S_{m.f}$ in the equations (7-9). This calculation process is iterated until the difference between the two consecutive values of J is negligible.

Thermal efficiency is an important aspect of the DCMD process of LiCl solutions as the regeneration step contributes over three quarters of the energy consumption of LDAC systems, and the energy consumption of the DCMD process is primarily attributed to thermal energy required for heating the feed stream. The thermal efficiency (Π) of the DCMD process is evaluated using the following equation (Alkhudhiri et al. 2012):

$$\Pi = \frac{J\Delta H_v}{J\Delta H_v + \frac{k_m}{\delta}(T_{m.f} - T_{m.d})} \tag{10}$$

Besides thermal efficiency, the specific thermal energy consumption (i.e. *STEC*) of the DCMD process of the LiCl solution is also assessed. *STEC* is the heating required to increase the weight concentration of one volume unit of LiCl solution feed by 1%, and can be calculated as:

$$STEC = \frac{m_{f.in} \times C_p \times (T_{f.in} - 25)}{3.6 \times 10^3 \times \Delta S \times V_{f.in}} \tag{11}$$

where *STEC* is in kWh/(%·m^3); m_{fin} is the feed inlet mass flow rate (kg/h); C_p is the specific heat capacity of the LiCl solution feed (kJ/(kg·°C)); $T_{f.in}$ is the feed inlet temperature of the DCMD process; ΔS is the LiCl concentration enrichment (i.e. the difference between the LiCl concentration at the outlet and the inlet of the feed channel) (%); and $V_{f.in}$ is the feed inlet volume flow rate (m^3/h). It is necessary to note that while *STEC* offers a practical indicator for the DCMD process energy efficiency, Π demonstrates the proportion of the useful heat (i.e. that is associated with the transfer of water) to the total heat transfer from the feed to the distillate along the membrane leaf inside the DCMD membrane module. Moreover, the calculation of *STEC* for the DCMD process in this study differs from that normally reported for seawater MD desalination applications because the main product of the DCMD process in this study is the concentrated LiCl solution but not fresh water as for seawater desalination.

2.2. Simulation approach

The simulation package used in this study is developed based on the descriptive mass and heat transfer (DHMF) model that has been validated and reported in a previous study by Duong et al. (2020). One notable feature of this simulation package is the inclusion of both temperature and concentration polarisation effects in the mass and heat transfer analyses, and it allows for the simulation of the DCMD process of the LiCl solution under two flow modes: co-current and counter-current flow (Fig. 1). Details about the DHMF model and the calculation of heat and mass flux through each membrane area under the two flow modes can be found in the previous study by Duong et al. (2020).

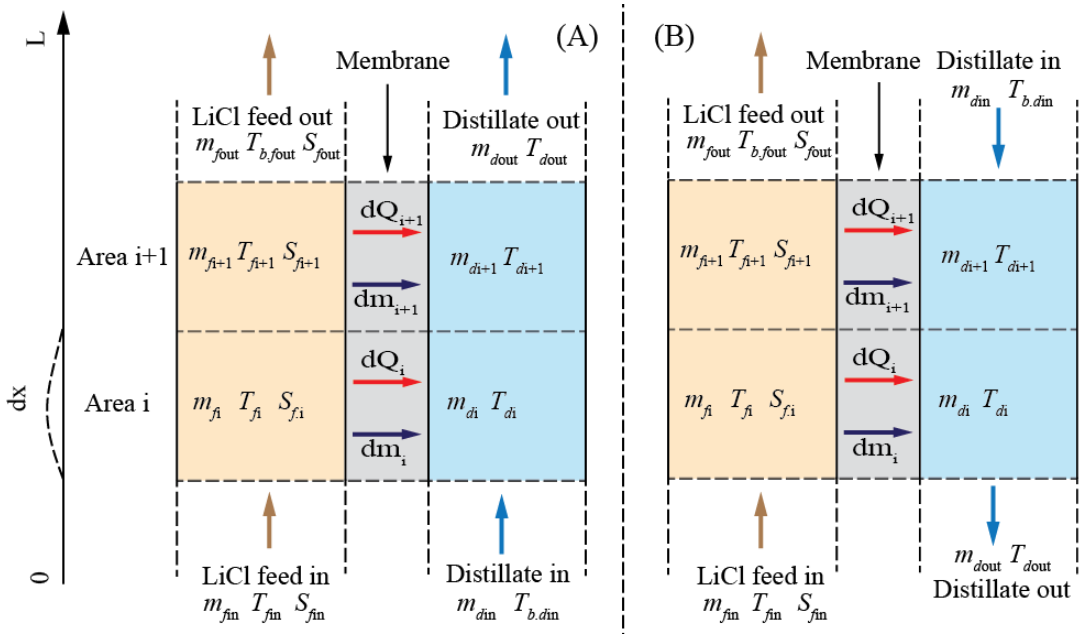

Fig. 1. Schematic diagram of two incremental membrane areas along the DCMD module under the (A) co-current and (B) counter-current flow mode.

The calculation algorithms of the DCMD process with the LiCl solution feed are illustrated in Fig. 2 and Fig. 3 for co-current and counter-current flow mode, respectively. The inputs of the calculation algorithms are the temperature, concentration, and mass flow rate of the LiCl solution feed and distillate respectively at the feed and distillate inlets (e.g. $T_{f.in}$, $S_{f.in}$, $m_{f.in}$, $T_{d.in}$, and $m_{d.in}$). The calculation starts from the feed inlet end (i.e. $x_0 = 0$) and finishes at the feed outlet end (i.e. $x_n = L$) of the DCMD module. For co-current flow, the initial parameters of the feed and distillate

streams are readily available. On the other hand, for counter-current flow, initial guesses of the mass flow and temperature of the distillate at the outlet (i.e. $m_{d.out}$ and $T_{d.out}$) are required (Fig. 3).

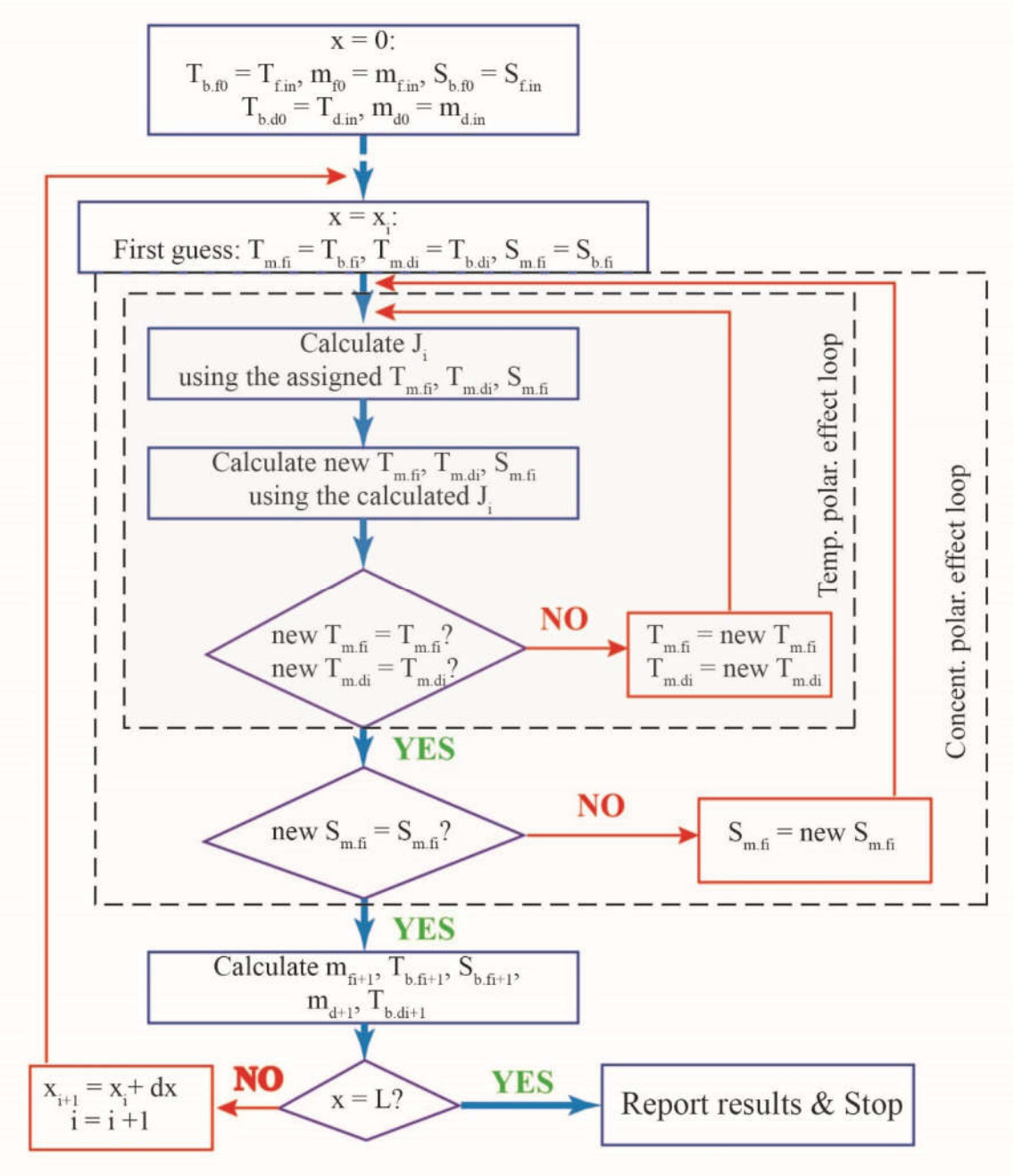

Fig. 2. Calculation algorithm of the DCMD simulation for co-current flow.

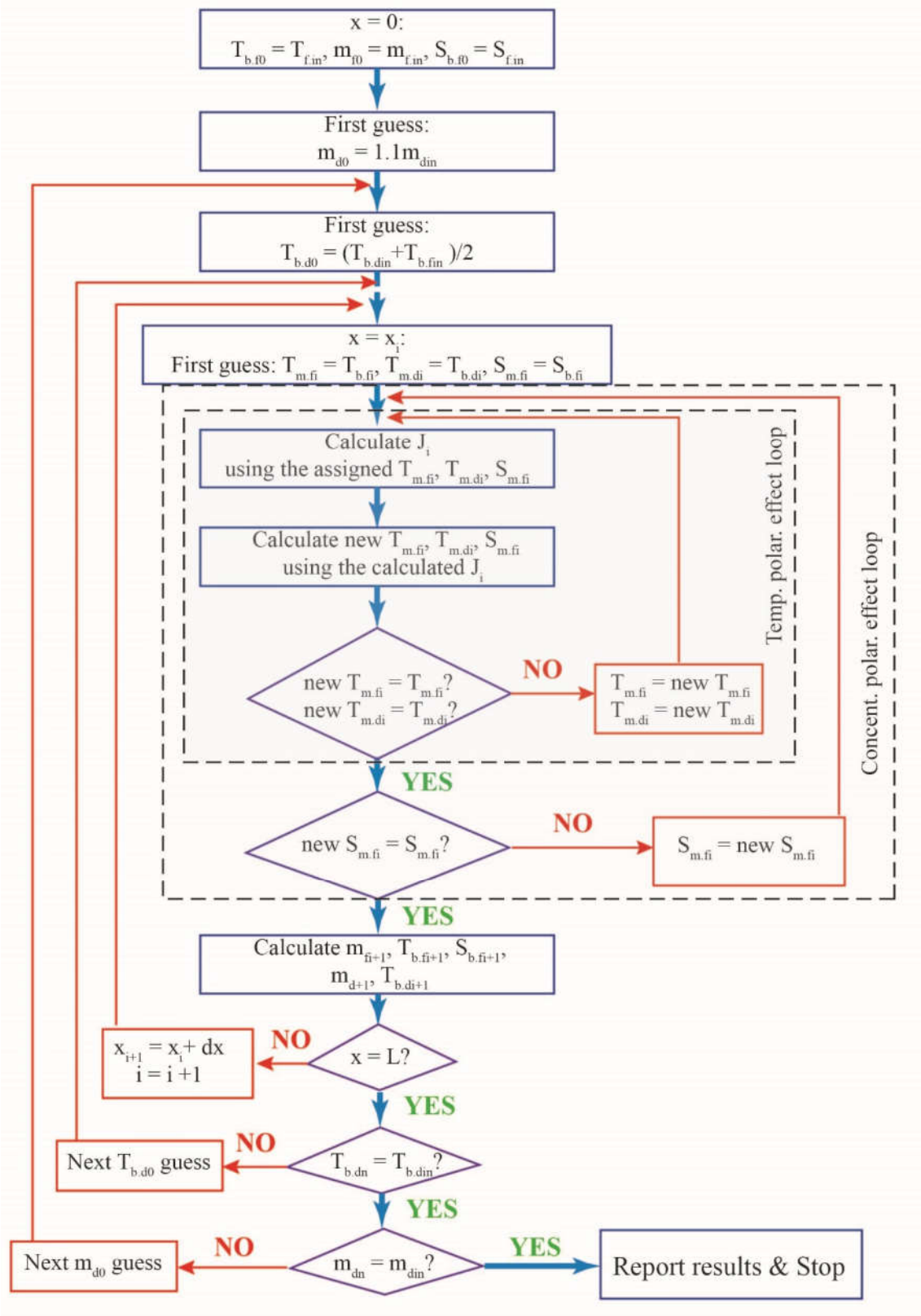

Fig. 3. Calculation algorithm of the DCMD simulation for counter-current flow.

277 The specifications of the membrane leaf and feed and distillate channels of the pilot DCMD
278 membrane module provided by AquaStill (Sittard, The Netherlands) (Hitsov et al. 2017) were used
279 for the simulation in this study. These specifications include membrane pore radius, membrane
280 porosity, membrane thickness, feed and distillate channel width and depth, and the membrane leaf
281 length. Unless otherwise stated, their default values are provided in Table 1. The pilot DCMD
282 membrane module used in (Hitsov et al. 2017) had six feed and six distillate channels, but they
283 were parallel. Thus, for simplicity the pilot DCMD membrane module simulated in this study is
284 composed of one feed and one distillate chanells with the same specifications.

285 **Table 1.** Specifications of the membrane leaf and flow channels of the pilot DCMD membrane
286 module

Membrane specifications	
Pore radius (μm)	0.15
Membrane porosity (–)	0.76
Membrane thickness (μm)	92
Feed and distillate channels	
Channel width (m)	0.4
Channel depth (m)	0.002
Channel length (m)	1.5

287 ## 3. Results and discussions

288 ### 3.1. Mass and heat transfer through the membrane inside the module

289 In the pilot DCMD regeneration of liquid desiccant LiCl solution, the flow mode exerts decisive
290 influence on the heat and mass transfer through the membrane. As demonstrated in Fig. 4, co-
291 current and counter-current modes result in two different feed and distillate temperatures and water
292 flux profiles inside the membrane module. Under the co-current flow mode, from the inlet to the
293 outlet of the membrane module the membrane surface feed temperature ($T_{m.f}$) declines while the
294 membrane surface distillate temperature ($T_{m.d}$) increases due to heat transferred from the feed to
295 the distillate, leading to a decrease in the transmembrane water temperature difference (i.e. ΔT_m)
296 (Fig. 4A). This decreased ΔT_m together with the increase in the LiCl concentration along the
297 membrane results in a rapid decline in local water flux (J) inside the membrane module from the
298 inlet to the outlet. Moreover, it is noteworthy that after the membrane length of 0.9 m, negative
299 water flux is observed despite the positive ΔT_m (>10 °C) (Fig. 4A). This finding confirms that the

actual driving force for water transfer through the membrane in MD is the transmembrane water vapour pressure (i.e. ΔP_m), not the transmembrane water temperature difference (ΔT_m). After the membrane length of 0.9 m, $T_{m.f}$ remains markedly higher than $T_{m.d}$; however, the water vapour pressure at the feed membrane surface is lower than that at the distillate membrane surface due to the hyper salinity of the LiCl solution. As a result, reverse water flux from the distillate to the LiCl solution feed occurs after the membrane length of 0.9 m (Fig. 4A).

On the other hand, the feed and distillate temperatures at the membrane surfaces and in the bulk streams linearly decrease from the feed inlet to the feed outlet of the membrane module under the counter-current mode (Fig. 4B). Although the temperature difference between the feed and distillate membrane surfaces (ΔT_m) remains largely constant along the membrane leaf, the local water flux markedly declines from the feed inlet to the feed outlet. The declining water flux along the membrane module under counter-current mode has been elucidated in the previous study by Duong et al. (2020) using a lab-scale membrane module. It is noteworthy that the local water flux declines at a higher rate near the feed inlet than toward the feed outlet due to the exponential relation between the water vapour pressure and the temperature of solutions (Fig. 4B).

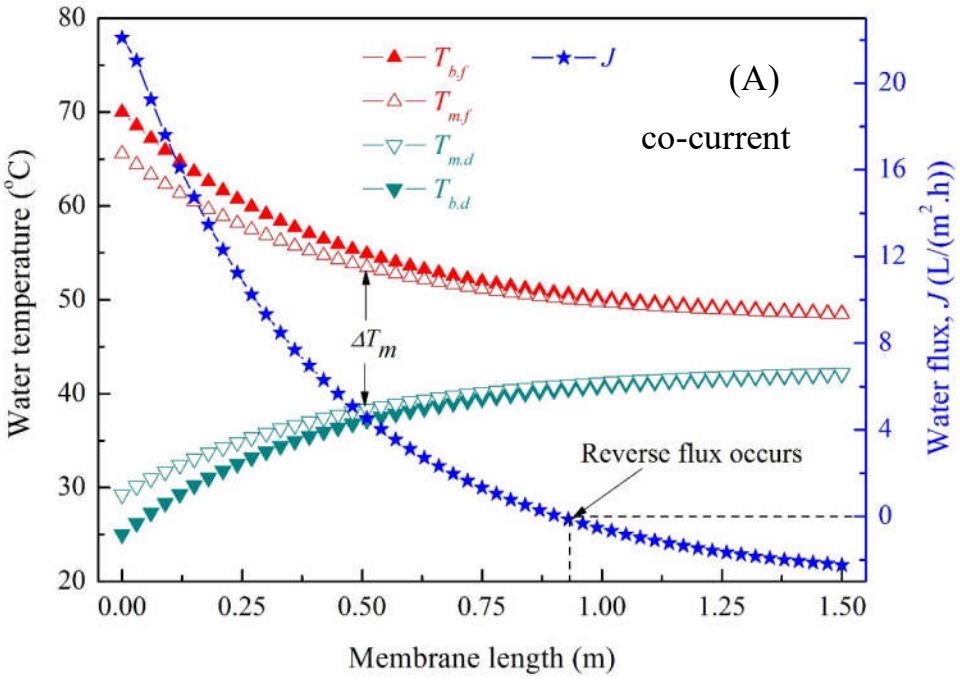

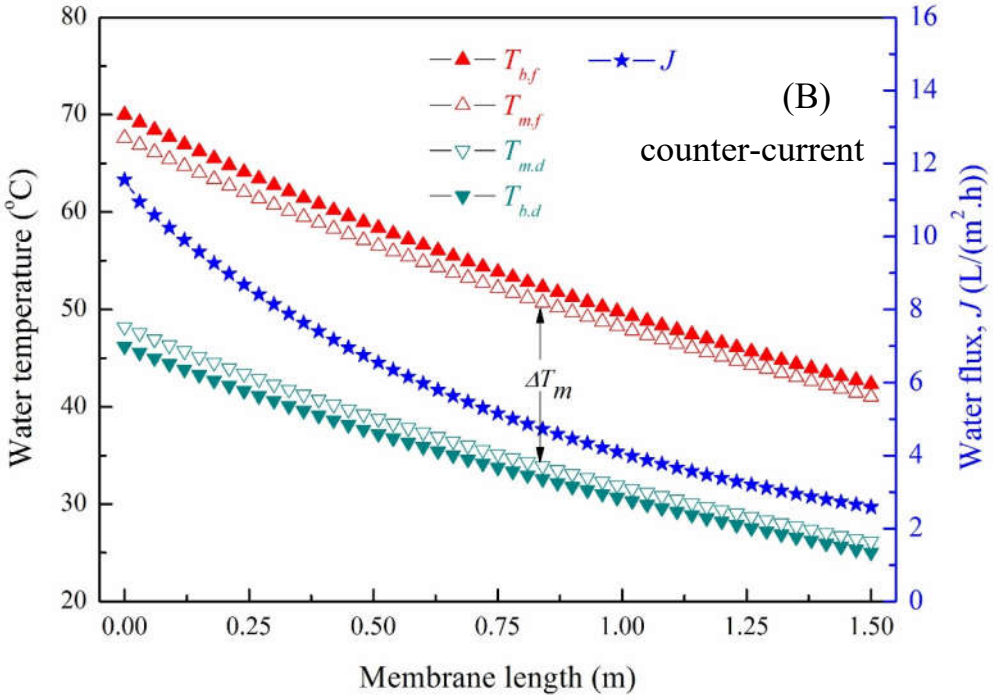

Fig. 4. Feed and distillate temperature at the membrane surfaces and in the bulk streams and water flux along the membrane inside the module during the DCMD regeneration of the LiCl 20% solution under (A) co-current and (B) counter-current flow. Operating conditions: feed inlet temperature ($T_{f.in}$) = 70 °C, distillate inlet temperature $T_{d.in}$ = 25 °C, feed and distillate inlet circulation rate $F_{f.in} = F_{d.in}$ = 250 L/h.

The discrepancy in local water flux inside the membrane module under the two operation modes results in noticeably different profiles of thermal efficiency and the LiCl solution concentration (Fig. 5). The thermal efficiency of the DCMD process with the LiCl 20% solution feed under both operation modes is mostly below 0.5. This means that during the DCMD regeneration of the LiCl 20% solution feed using the pilot system, more than half of the heat transfer from the feed to the distillate is due to the heat conduction through the membrane and is deemed the heat loss. Furthermore, thermal efficiency under co-current mode is discernibly lower than that under the counter-current mode, demonstrating that the counter-current operation is more beneficial to the pilot DCMD regeneration of LiCl solution with respect to thermal efficiency. It is important to stress that previous experimental studies on lab-scale DCMD regeneration of liquid desiccant LiCl solutions have not investigated the process thermal efficiency.

The bulk LiCl concentration (i.e. $S_{b,f}$) profiles along the membrane leaf under the two flow modes also clearly differ (Fig. 5). Under the co-current flow, from the feed inlet the LiCl concentration steadily increases and maximizes at the membrane length of 0.9 m before gradually

decreasing toward the feed outlet (i.e. 1.5 m). On the other hand, the LiCl concentration under the counter-current mode progressively rises from the feed inlet to the feed outlet (Fig. 5). Indeed, these LiCl concentration profiles are consistent with the water flux profiles shown in Fig. 4. The decreased LiCl concentration under the co-current flow after the membrane length of 0.9 m is due to the negative water flux (Fig. 4A). Moreover, the LiCl concentration at the feed outlet under the counter-current flow is noticeably higher than that under the co-current mode. This also manifests the advantage of the counter-current operation over the co-current one for the pilot DCMD regeneration of LiCl solutions.

The analysis of heat and mass transfer through the membrane inside the module has revealed the superiority of the counter-current to the co-current mode during the pilot DCMD regeneration of the liquid desiccant LiCl solution. Thus, the counter-current mode is selected for further investigations on the influences of the operating conditions and membrane length on the pilot DCMD process performance discussed in the next section.

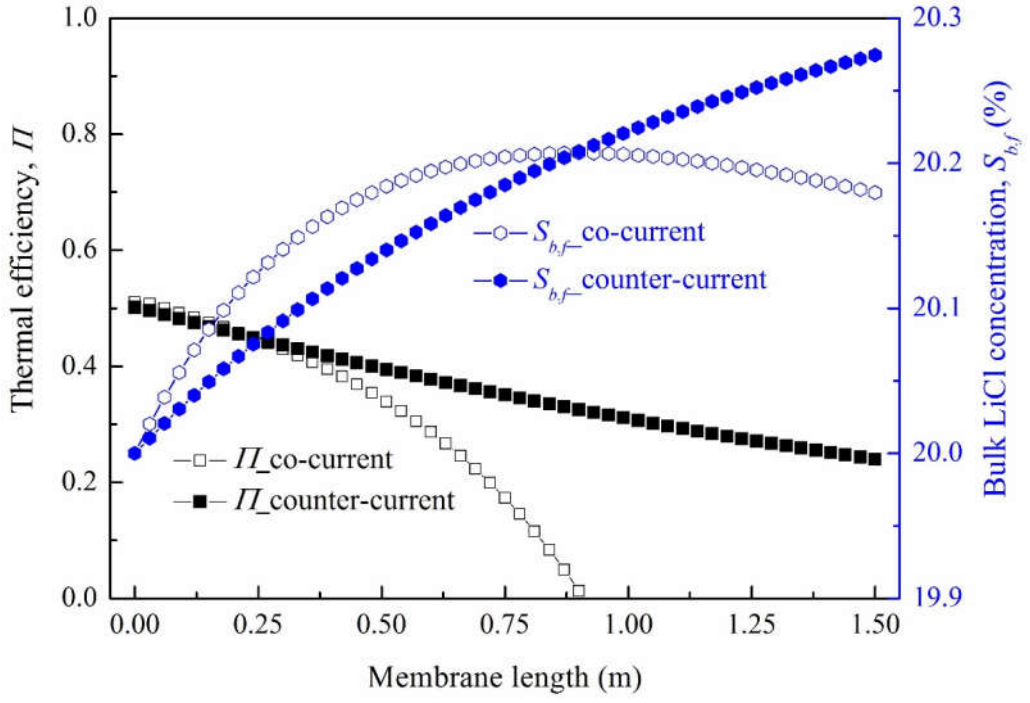

Fig. 5. Thermal efficiency and the bulk LiCl concentration along the membrane inside the module during the DCMD regeneration of the LiCl 20% solution under co-current and counter-current flow. Operating conditions: feed inlet temperature ($T_{f.in}$) = 70 °C, distillate inlet temperature $T_{d.in}$ = 25 °C, feed and distillate inlet circulation rate $F_{f.in}$ = $F_{d.in}$ = 250 L/h.

3.2. Influences of operating conditions on the DCMD process performance

The key operating conditions of the pilot DCMD regeneration of LiCl solutions include the feed inlet temperature, the feed and distillate circulation rate, and the inlet LiCl concentration. The distillate inlet temperature has less influence on the DCMD process performance; thus, it is fixed at 25 °C in all simulations. The performance of the DCMD regeneration of LiCl solutions is assessed using the process water flux ($J_{process}$), thermal efficiency ($\Pi_{process}$), specific thermal energy consumption (*STEC*), and the increase in the LiCl concentration from the inlet to the outlet (i.e. ΔS). While *STEC* is calculated using equation (11), $J_{process}$ and $\Pi_{process}$ are the average values of local water flux (J) and thermal efficiency (Π) along the membrane leaf.

The simulation results reveal that it is beneficial to operate the pilot DCMD process of LiCl solutions at higher feed inlet temperature and higher water circulation rates. As demonstrated in Fig. 6A, elevating the feed inlet temperature boosts both $J_{process}$ and $\Pi_{process}$ while substantially reducing *STEC* of the DCMD process. Increasing feed and distillate circulation rates also favours the improvement of the $J_{process}$ and $\Pi_{process}$ and the reduction in *STEC* (Fig. 6B), but at a lower extent compared to elevating the feed inlet temperature. Indeed, the benefits of operating the DCMD process of LiCl solution at high feed inlet temperature and water circulation rates have been proven in experimental works using lab-scale units (Duong et al. 2017; Duong et al. 2018). The results reported here, however, highlight that even under the optimal feed inlet temperature and water circulation rates, the pilot DCMD regeneration of LiCl solutions exhibits limited thermal efficiency (i.e. $\Pi_{process}$ <0.5) and discernibly high *STEC* (i.e. ~100 kWh/(%.m^3)). The poor thermal efficiency of the DCMD process with the LiCl solution can be attributed to the hyper salinity of the LiCl solution feed.

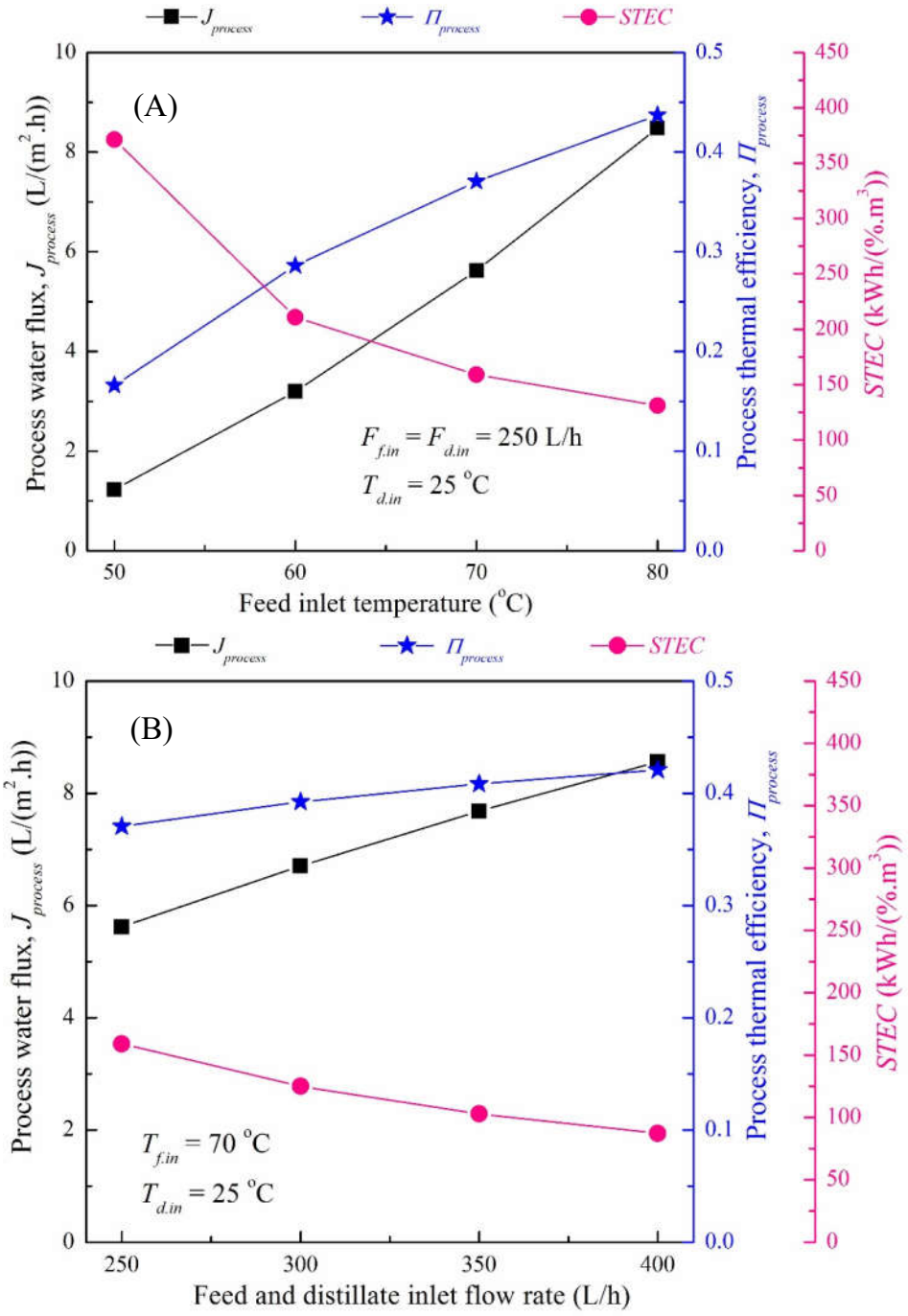

374 **Fig. 6.** The process water flux ($J_{process}$), process thermal efficiency ($\Pi_{process}$), and specific thermal
375 energy consumption (*STEC*) of the DCMD regeneration of the LiCl 20% solution at (A) different
376 feed inlet temperature and (B) different feed and distillate flow rate under counter-current flow.
377 Other operating conditions: distillate inlet temperature $T_{d.in}$ = 25 °C.

378 The inlet LiCl concentration profoundly affects the performance of the DCMD process (Fig.
379 7). When the inlet LiCl concentration is elevated from 20% to 30%, $J_{process}$ reduces by 91% from

5.6 to 0.5 L/(m^2·h), coinciding with a reduction in the $\Pi_{process}$ by 89% (i.e. from 0.37 to 0.04). The LiCl concentration regulates not only the water vapour pressure but also the thermodynamic properties (i.e. particularly the viscosity) of the feed solution, thus restraining the mass transfer coefficient and water vapour flux through the membrane. Indeed, the simulation results reveal that the dynamic viscosity of the LiCl solution doubles when the LiCl concentration is increased from 20% to 30%. Previous experimental lab-scale works have demonstrated the strong impacts of the feed concentration on water flux during the DCMD regeneration of LiCl solutions (Duong et al. 2017; Duong et al. 2018). These impacts are even more profound for the pilot DCMD process of LiCl solutions given its much longer membrane leaf compared to that used in the lab-scale units. The effects of membrane leaf length on the water flux and hence the thermal efficiency of the pilot DCMD process with LiCl solution will be further elucidated in section 3.3. The limited water flux and poor thermal efficiency inevitably leads to the discernibly high values of *STEC* at higher inlet LiCl concentration (Fig. 7).

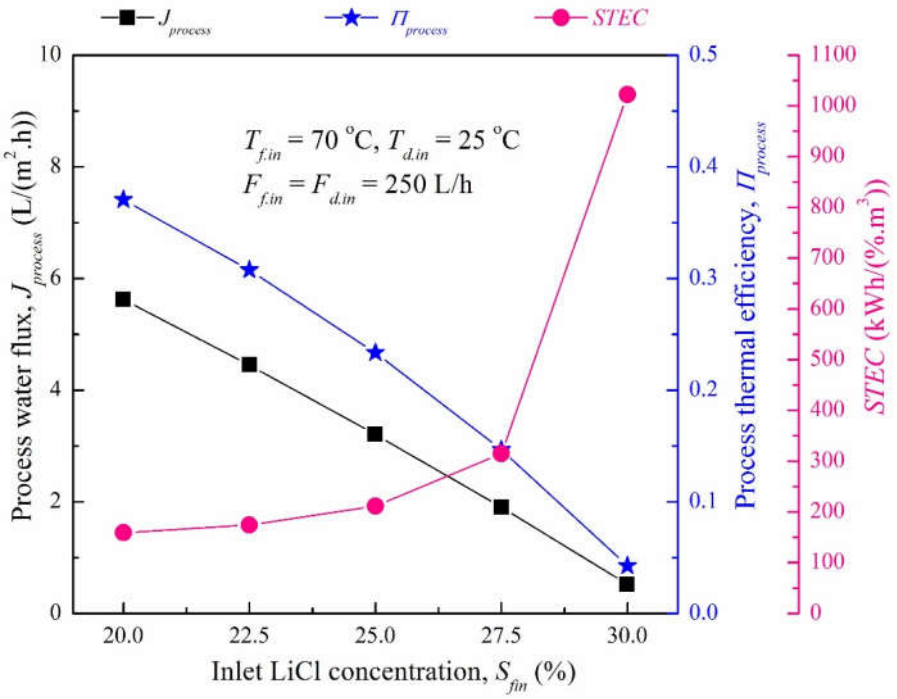

Fig. 7. The process water flux ($J_{process}$), thermal efficiency ($\Pi_{process}$), and specific thermal energy consumption (*STEC*) of the DCMD process of the LiCl solution at different concentration. Other operating conditions: feed inlet temperature ($T_{f.in}$) = 70 °C, distillate inlet temperature $T_{d.in}$ = 25 °C, feed and distillate inlet circulation rate $F_{f.in}$ = $F_{d.in}$ = 250 L/h.

Another important indicator for the performance of the DCMD regeneration of LiCl solutions is the enrichment of LiCl in the feed (i.e. ΔS). The three key operating conditions (e.g. feed inlet temperature, water circulation rate, and the inlet LiCl concentration) exhibit different effects on ΔS (Fig. 8). The feed inlet temperature is proportional with ΔS while elevating the LiCl solution concentration noticeably reduces ΔS (Fig. 8A&B). The impacts of feed inlet temperature and the LiCl concentration on ΔS appear similarly to their effects on water flux shown in Fig. 6A and Fig. 7. On the other hand, the feed and distillate circulation rates exert negligible impacts on ΔS despite having a linear relationship with water flux (Fig. 6B). Unlike the feed inlet temperature and the LiCl concentration, the feed and distillate circulation rates determine the retention time of the LiCl solution inside the membrane module. Increasing the water circulation rates enhances water flux but also shortens the retention time of the LiCl solution feed. As a result, the impacts of the feed and distillate circulation rates on ΔS seem to be neutralized (Fig. 8C).

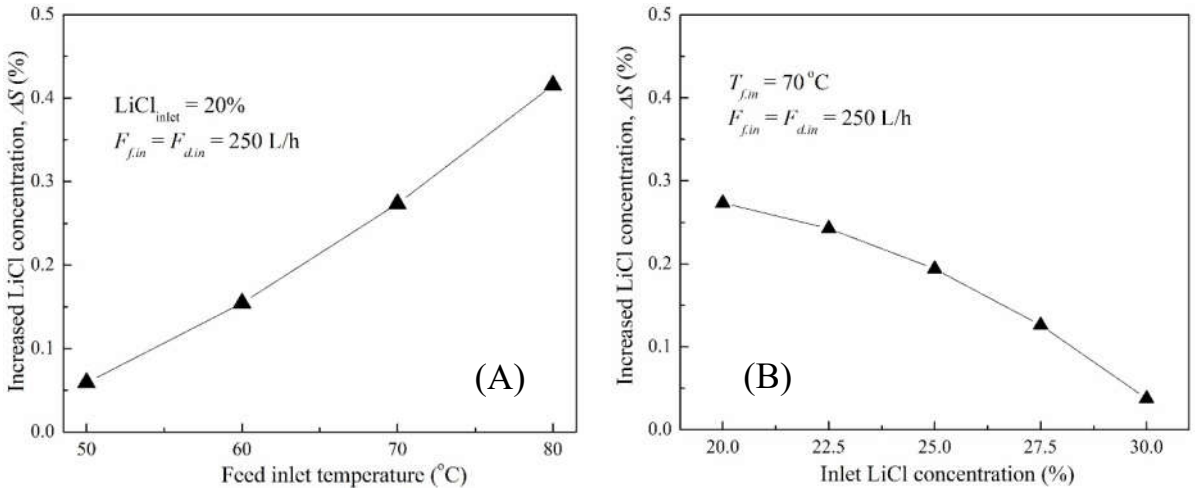

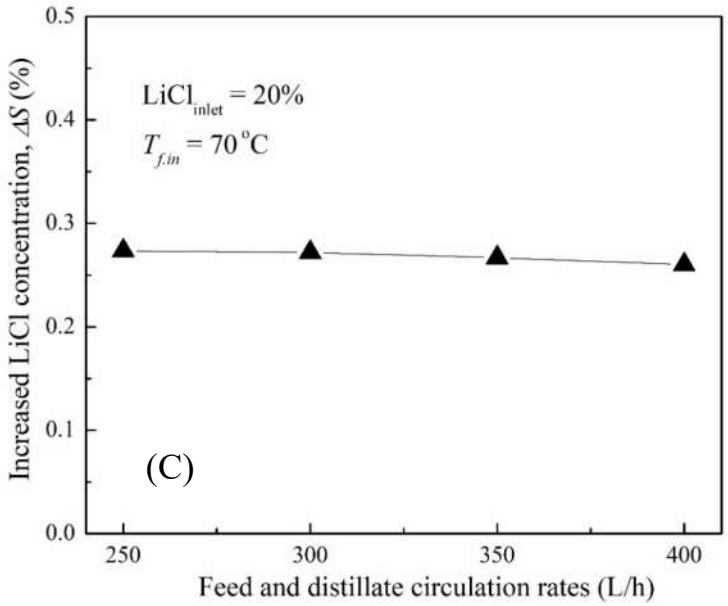

Fig. 8. The LiCl concentration enrichment achieved during the DCMD regeneration of the LiCl solution at various (A) feed inlet temperature, (B) inlet LiCl concentration, and (C) feed and distillate water circulation rates under counter-current flow. Other operating conditions: distillate inlet temperature $T_{d.in}$ = 25 °C.

3.3. Influences of the membrane length on the DCMD process performance

Unlike experimental works using lab-scale units with fix membrane module specifications, the simulation in this study allows for systematically assessing the influences of membrane module specifications on the performance of the pilot DCMD regeneration of LiCl solutions. One of the most critical membrane module specifications for the pilot DCMD process is the membrane leaf length.

The simulation results reveal that the pilot DCMD process with LiCl solutions is more efficient when using a shorter membrane leaf (Fig. 9). The process with the shorter membrane leaf achieves higher water flux and thermal efficiency but lower *STEC* under the same operating conditions (e.g. feed inlet temperature, feed and distillate circulation rate, and inlet LiCl concentration). The enhanced process performance with the shortened membrane leaf can be attributed to the increased transmembrane temperature difference (i.e. ΔT_m). For example, at the feed inlet and the distillate inlet temperatures of 70 °C and 25 °C, feed and distillate circulation rate of 250 L/h, and the inlet LiCl concentration of 20%, the average ΔT_m of the process with the membrane length of 0.5 m and 1.5 m is 25.5 °C and 17.1 °C, respectively. Given the exponential relation between the water vapour

pressure and the temperature, the reduction in ΔT_m when increasing the membrane leaf length inevitably leads to the decline in water flux (Fig. 9). This decreasing water flux in turn negatively affects thermal efficiency ($\Pi_{process}$) and hence raises the *STEC* of the process.

The results reported here have important implications to the design of the membrane modules destined for liquid desiccant air-conditioning applications. Membrane modules with longer membrane leaves offer larger membrane areas for water evaporation and hence achieve a higher LiCl concentration at the outlet of the membrane modules. However, the process using longer membrane exhibits lower water flux and thermal efficiency as discussed above. Therefore, for the pilot DCMD regeneration of liquid desiccant solutions, it is more beneficial to deploy membrane modules with short membrane leaves. The process can be operated in batch mode or brine recycling mode (i.e. whereby the brine leaving the membrane modules is returned to the feed tank for further treatment cycles) (Duong et al. 2015; Duong et al. 2017). Operating under these modes, the LiCl concentration can be achieved without compromising the water flux and thermal efficiency of the pilot DCMD process.

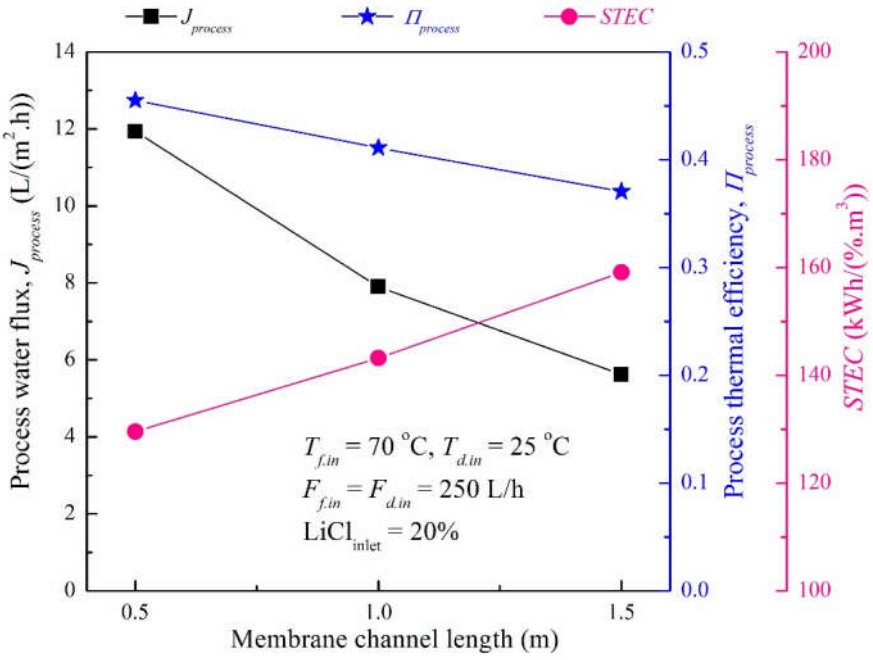

Fig. 9. The process water flux ($J_{process}$), thermal efficiency ($\Pi_{process}$), and specific thermal energy consumption (*STEC*) of the pilot DCMD regeneration of the LiCl 20% solution using the membrane module with different membrane length. Other operating conditions: feed inlet temperature ($T_{f.in}$) = 70 °C, distillate inlet temperature $T_{d.in}$ = 25 °C, feed and distillate inlet circulation rate $F_{f.in}$ = $F_{d.in}$ = 250 L/h.

4. Conclusions

This study assesses the pilot DCMD regeneration of liquid desiccant LiCl solution in LDAC systems using computer simulation. In contrast to experimental investigations, the simulation allows for the insightful evaluation of the heat and mass transfer through the membrane inside the DCMD membrane module as it can incorporate both temperature and concentration polarisation effects in the calculation of heat and water flux. The simulation results demonstrate that the flow mode of the pilot DCMD process strongly affects the heat and mass transfer across the membrane, and the counter-current flow mode is more beneficial than co-current one regarding the process water flux, thermal efficiency, and LiCl concentration enrichment. Moreover, when operating the pilot DCMD process of LiCl solution under the counter-current flow, the feed inlet temperature, the feed LiCl concentration, and particularly the membrane leaf length are significant factors governing the process performance. When increasing the membrane leaf length from 0.5 to 1.5 m, the process water flux decreases by a half from 12 to 6 L/(m^2·h) and thermal efficiency decreases by 20%. These simulation results have important implications to the design of the pilot DCMD membrane modules, particularly the membrane leaf length.

Acknowledgements

This research is funded by Vietnam National Foundation for Science and Technology Development (NAFOSTED) under the grant number 105.08-2019.08.

References

Abdelkader S, Gross F, Winter D, Went J, Koschikowski J, Geissen SU, and Bousselmi L (2019) Application of direct contact membrane distillation for saline dairy effluent treatment: performance and fouling analysis. Environ. Sci. Pollut. Res. 26:18979-18992.

Alkhudhiri A, Darwish N, and Hilal N (2012) Membrane distillation: A comprehensive review. Desalination 287:2-18.

Andrés-Mañas JA, Roca L, Ruiz-Aguirre A, Acién FG, Gil JD, and Zaragoza G (2020) Application of solar energy to seawater desalination in a pilot system based on vacuum multi-effect membrane distillation. Appl. Energy 258:114068.

476 Andrés-Mañas JA, Ruiz-Aguirre A, Acién FG, and Zaragoza G (2018) Assessment of a pilot
477 system for seawater desalination based on vacuum multi-effect membrane distillation with
478 enhanced heat recovery. Desalination 443:110-121.

479 Anvari A, Azimi Yancheshme A, Kekre KM, and Ronen A (2020) State-of-the-art methods for
480 overcoming temperature polarization in membrane distillation process: A review. J. Membr. Sci.
481 616:118413.

482 Bindels M, Carvalho J, Gonzalez CB, Brand N, and Nelemans B (2020) Techno-economic
483 assessment of seawater reverse osmosis (SWRO) brine treatment with air gap membrane
484 distillation (AGMD). Desalination 489:114532.

485 Chen X, Riffat S, Bai H, Zheng X, and Reay D (2020) Recent progress in liquid desiccant
486 dehumidification and air-conditioning: A review. Energ. Built Environ. 1:106-130.

487 Cheng Q and Zhang X (2013) Review of solar regeneration methods for liquid desiccant air-
488 conditioning system. Energ. Buildings 67:426-433.

489 Conde MR (2004) Properties of aqueous solutions of lithium and calcium chlorides: formulations
490 for use in air conditioning equipment design. Int. J. Therm. Sci. 43:367-382.

491 Dong G, Kim JF, Kim JH, Drioli E, and Lee YM (2017) Open-source predictive simulators for
492 scale-up of direct contact membrane distillation modules for seawater desalination. Desalination
493 402:72-87.

494 Duong HC, Álvarez IRC, Nguyen TV, and Nghiem LD (2018) Membrane distillation to regenerate
495 different liquid desiccant solutions for air conditioning. Desalination 443:137-142.

496 Duong HC, Ansari AJ, Cao HT, Nguyen NC, Do KU, and Nghiem LD (2020) Membrane
497 distillation regeneration of liquid desiccant solution for air-conditioning: Insights into polarisation
498 effects and mass transfer. Environ. Technolo. Inno. 19:100941.

499 Duong HC, Ansari AJ, Nghiem LD, Cao HT, Vu TD, and Nguyen TP (2019) Membrane Processes
500 for the Regeneration of Liquid Desiccant Solution for Air Conditioning. Curr. Pollut. Rep. 5:308-
501 318.

502 Duong HC, Cooper P, Nelemans B, Cath TY, and Nghiem LD (2015) Optimising thermal
503 efficiency of direct contact membrane distillation by brine recycling for small-scale seawater
504 desalination. Desalination 374:1-9.

505 Duong HC, Hai FI, Al-Jubainawi A, Ma Z, He T, and Nghiem LD (2017) Liquid desiccant lithium
506 chloride regeneration by membrane distillation for air conditioning. Sep. Purif. Technol. 177:121-
507 128.

508 Duong HC, Pham TM, Luong ST, Nguyen KV, Nguyen DT, Ansari AJ, and Nghiem LD (2019) A
509 novel application of membrane distillation to facilitate nickel recovery from electroplating
510 wastewater. Environ. Sci. Pollut. Res. 26:23407-23415.

511 Duong HC, Xia L, Ma Z, Cooper P, Ela W, and Nghiem LD (2017) Assessing the performance of
512 solar thermal driven membrane distillation for seawater desalination by computer simulation. J.
513 Membr. Sci. 542:133-142.

514 Gurubalan A, Maiya MP, and Geoghegan PJ (2019) A comprehensive review of liquid desiccant
515 air conditioning system. Appl. Energy 254:113673.

516 Hitsov I, Eykens L, Schepper WD, Sitter KD, Dotremont C, and Nopens I (2017) Full-scale direct
517 contact membrane distillation (DCMD) model including membrane compaction effects. J. Membr.
518 Sci. 524:245-256.

519 Hitsov I, Maere T, De Sitter K, Dotremont C, and Nopens I (2015) Modelling approaches in
520 membrane distillation: A critical review. Sep. Purif. Technol. 142:48-64.

521 Khayet M, Velázquez A, and Mengual JI (2004) Modelling mass transport through a porous
522 partition: Effect of pore size distribution. J. Non-Equil. Thermody. 29:279-299.

523 Kuang Z, Long R, Liu Z, and Liu W (2019) Analysis of temperature and concentration
524 polarizations for performance improvement in direct contact membrane distillation. Int. J. Heat
525 Mass Tran. 145:118724.

526 Lefers R, Bettahalli NMS, Fedoroff N, Nunes SP, and Leiknes T (2018) Vacuum membrane
527 distillation of liquid desiccants utilizing hollow fiber membranes. Sep. Purif. Technol. 199:57-63.

528 Liu J, Ren H, Hai FI, Albdoor AK, and Ma Z (2021) Direct contact membrane distillation for liquid
529 desiccant regeneration and fresh water production: Experimental investigation, response surface
530 modeling and optimization. Appl. Therm. Eng. 184:116293.

531 Lokare OR, Ji P, Wadekar S, Dutt G, and Vidic RD (2019) Concentration polarization in membrane
532 distillation: I. Development of a laser-based spectrophotometric method for in-situ
533 characterization. J. Membr. Sci. 581:462-471.

534 Lowenstein A (2008) Review of Liquid Desiccant Technology for HVAC Applications. HVAC&R
535 Research 14:819-839.

536 Modi KV and Shukla DL (2018) Regeneration of liquid desiccant for solar air-conditioning and
537 desalination using hybrid solar still. Energy Convers. Manag. 171:1598-1616.

538 Nguyen NC, Chen S-S, Jain S, Nguyen HT, Ray SS, Ngo HH, Guo W, Lam NT, and Duong HC
539 (2018) Exploration of an innovative draw solution for a forward osmosis-membrane distillation
540 desalination process. Environ. Sci. Pollut. Res. 25:5203-5211.

541 Salikandi M, Ranjbar B, Shirkhan E, Shanmuga Priya S, Thirunavukkarasu I, and Sudhakar K
542 (2021) Recent trends in liquid desiccant materials and cooling systems: Application, performance
543 and regeneration characteristics. J. Build. Eng. 33:101579.

544 Yan Z, Yang H, Qu F, Yu H, Liang H, Li G, and Ma J (2017) Reverse osmosis brine treatment
545 using direct contact membrane distillation: Effects of feed temperature and velocity. Desalination
546 423:149-156.

547 Zhou J, Noor N, Wang F, and Zhang X (2020) Simulation and experiment on direct contact
548 membrane distillation regenerator in the liquid dehumidification air-conditioning system. Build.
549 Environ. 168:106496.

550 Zhou J, Wang F, Noor N, and Zhang X (2020) An experimental study on liquid regeneration
551 process of a liquid desiccant air conditioning system (LDACs) based on vacuum membrane
552 distillation. Energy 194:116891.

553 Zhou J, Zhang X, Su W, and Sun B (2019) Performance analysis of vacuum membrane distillation
554 regenerator in liquid desiccant air conditioning system. Int. J. Refrig.102:112-121.